AFM Imaging of Mercaptobenzoic Acid on Au(110): Sub-Molecular Contrast with Metal Tips

Nadine Hauptmann,[*,†,‖] Roberto Robles,[‡] Paula Abufager,[¶] Nicolas Lorente,[§] and Richard Berndt[†]

†*Institut für Experimentelle und Angewandte Physik, Christian-Albrechts-Universität zu Kiel, 24098 Kiel, Germany*

‡ *Catalan Institute of Nanoscience and Nanotechnology (ICN2), CSIC and The Barcelona Institute of Science and Technology, Campus UAB, Bellaterra, 08193 Barcelona, Spain*

¶*Instituto de Física de Rosario, Consejo Nacional de Investigaciones Científicas y Técnicas (CONICET) and Universidad Nacional de Rosario, Av. Pellegrini 250 (2000) Rosario, Argentina*

§*Centro de Física de Materiales CFM/MPC (CSIC-UPV/EHU), Paseo Manuel de Lardizabal 5, 20018 Donostia-San Sebastián, Spain*

& Donostia International Physics Center (DIPC), Paseo Manuel de Lardizabal 4, 20018 Donostia-San Sebastián, Spain

‖*Current address: Institute for Molecules and Materials, Radboud University, 6500 GL Nijmegen, The Netherlands*

E-mail: n.hauptmann@science.ru.nl

Abstract

A self-assembled monolayer of mercaptobenzoic acid (MBA) on Au(110) is investigated with scanning tunneling and atomic force microscopy (STM, AFM) and density functional calculations. High-resolution AFM images obtained with metallic tips show clear contrasts between oxygen atoms and phenyl moieties. The contrast above the oxygen atoms is due to attractive covalent interactions which is different from previously reported high-resolution images where Pauli repulsion dominated the image contrast. We show that the bonding of MBA to the substrate occurs mainly through dispersion interactions while the thiol-Au bond contributes only a quarter of the adsorption energy. No indication of Au adatoms mediating the thiol-Au interaction was found in contrast to other thiol-bonded systems. However, MBA lifts the Au(110)-(2×1) reconstruction.

Graphical TOC Entry

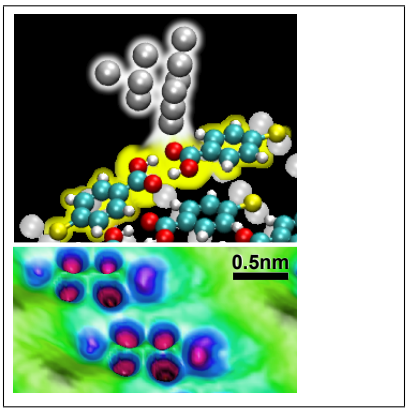

Combined scanning tunneling and atomic force microscopy (STM and AFM) delivers information on molecular structures and chemical interactions on the atomic scale. The method was used for sub-molecular resolution imaging of pure hydrocarbons[1–6] as well as other carbon-based molecules like fullerenes[7–10] or π-conjugated polymers.[11] In nearly all of these works, the tip of the scanning tunneling microscope was functionalized by a single CO molecule. The observed sharply localized contrasts are interpreted in terms of Pauli repulsion and the bendability of the bond between CO and the tip apex atom.[12,13] Recently, molecules comprising heteroatoms have been addressed.[14–24] As soon as electrostatic dipoles in the molecule or tip are present, the electrostatic force plays an important role in interpreting the images.[20,22,24–27]

Thiols are of great interest owing to their capacity to self-assemble and to create various structures thanks to their functionalizing groups.[28] The adsorption of thiols on Au(111) has been investigated over a range of coverages using a variety of methods including STM and X-ray diffraction.[29–34] There is consensus concerning the observed structural 2-dimensional phases,[35–41] but the discussion about involved Au adatoms at the S-Au interface is still ongoing.[42] Among the thiol-based molecules, 4-Mercaptobenzoic acid (MBA) has received particular attention because it led to the unraveling of thiol-gold structures based on an adatom model on gold nanoclusters.[43–45] However, no adatoms appeared to be involved in the formation MBA monolayers on Au(111).[46] The structural phases of MBA monolayers are similar as for other thiols according to X-ray photoelectron spectroscopy[47,48] and STM data.[46,49] However, a recent STM study of a MBA related molecule (4-mercaptopyridine) on Au(111) suggested an upright orientation at low coverages[50] where other thiols lie flat on the substrate. Indeed, MBA is an intriguing molecule despite its simple structure. It consists of a phenyl ring with a π-electron system that gives rise to interesting van der Waals interaction and molecular stacking in crystals. In addition, its carboxyl group leads to hydrogen-bonding while the thiol group provides covalent binding to metal atoms.

Here, we use high-resolution AFM and STM to image arrays of MBA with metallic tips.

High-resolution images are obtained at tip–sample distances where the molecules cause an increased attraction. The oxygen atoms appear as remarkably sharp features in frequency-shift AFM images. This chemical contrast provided by metallic tips is different from the results mentioned above that involved functionalized tips. Moreover, repulsive force contributions were identified as the origin of the sub-molecular resolution. We disentangle the various forces acting on MBA by means of density functional theory (DFT) calculations, which show that a covalent interaction of the metallic tip with the oxygen atoms is predominant. An electrostatic force is present but less important. Concerning the adsorption of MBA on the Au(110) surface we find that the molecules form a zigzag pattern of dimers that are due to hydrogen bonding of the carboxylic groups. Our calculations reveal that the dispersion interaction of π-electrons of the phenyl ring with the metal substrate is essential for the MBA-Au bond. The Au(110)-(2×1) reconstruction is lifted. The experimental data do not indicate an involvement of Au adatoms in binding the MBA molecules.

In constant-current STM images MBA molecules appear as elliptical protrusions on the Au(110) surface (Fig. 1(a) and (h)). At coverages of ≈ 0.3 monolayers (one monolayer being defined as a coverage of one molecule per five surface gold atoms) the molecules aggregate into compact islands. Within these islands the long axes of the ellipses are aligned along the [001] direction with spacings of (7.8 ± 0.3) Å and (12.3 ± 0.3) Å. A unit cell comprising four MBA molecules is depicted by a white rectangle in Fig. 1(a). Its dimensions of $(20.1 \pm 0.3) \times (10 \pm 1)$ Å^2 correspond to a (5×4) overlayer. The distances, sizes and corrugations in our measurements indicate that MBA molecules adsorb in a nearly planar orientation on Au(110), contrary to what has been reported for other surfaces.[46–50]

Further details of the molecular structure are resolved in constant height measurements of the tunneling current and the frequency shift. The tunneling-current map (Fig. 1(b)) shows an asymmetry of the molecular protrusions with maxima of the current localized close to the phenyl rings. In the frequency-shift map of Fig. 1(c), each molecule gives rise to three features. The frequency shift is negative in two well-defined spots and a more diffuse area.

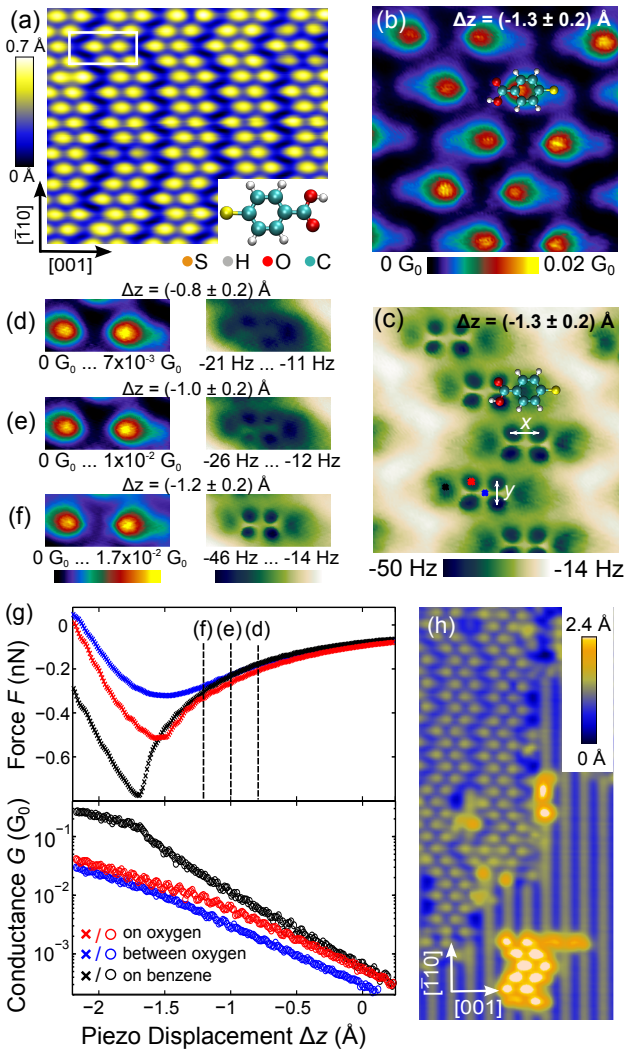

Figure 1: (a) STM topograph of an island of MBA molecules (structure model in the inset) on Au(110) (9.9 nm × 8.3 nm, sample voltage $V = 1$ V, tunneling current $I = 0.2$ nA, temperature 5.3 K). The white box indicates a unit cell. Maps of (b) the tunneling current and (c) the frequency shift (2.6 nm × 2.6 nm, $V = 15$ mV) simultaneously acquired at a constant tip height (piezo displacement $\Delta z = (-1.3 \pm 0.2)$ Å). Colored dots indicate the positions where the data shown in (g) was recorded. Structure models of MBA are overlaid for clarity. (d), (e), and (f) Current and frequency shift maps simultaneously acquired at different heights that are indicated in (g) (1.56 nm × 0.63 nm, $V = 14$ mV). (g) Short-range force and instantaneous conductance measured on three positions defined in (c). $\Delta z = 0$ Å corresponds to the tip–molecule distance above a benzene ring for an STM set-point of $I = 0.4$ nA and $V = 21$ mV. (h) Overview image of MBA islands (8.6 nm × 18.7 nm, $V = 26$ mV, $I = 0.3$ nA).

The distances between the sharp depressions are $y = (2.1 \pm 0.2)$ Å and $x = (2.8 \pm 0.2)$ Å. y matches the oxygen-oxygen distance in MBA. x is consistent with hydrogen bonding

between O atoms of adjacent molecules. Therefore, these spots are suggested to stem from the oxygen atoms while the diffuse areas, corresponding to the maxima in the current, are ascribed to the phenyl rings. The oxygen-induced features in the frequency shifts appear surprisingly sharp. Δf changes from ≈ -45 Hz to ≈ -23 Hz back to ≈ -40 Hz over a lateral distance of only 2.1 Å. As discussed below, we attribute the high resolution to an attractive interaction localized to the oxygen atoms.

As the tip approaches any part of the molecule, the force becomes increasingly attractive (Fig. 1(g)). The maximal force above the phenyl ring occurs at a slightly smaller tip–molecule distance (by ≈ 0.2 Å) than above or between the oxygen atoms. The absolute values of the maximal forces vary somewhat depending on the tip ($-0.8 \ldots -1.5$ nN above the phenyl ring, $-0.5 \ldots -1.1$ nN and $-0.3 \ldots -0.8$ nN, above and between O atoms, respectively), but systematically the force above the phenyl ring is more attractive than at any other position. Compared to forces obtained with CO tips, the present force values are roughly one order of magnitude larger.[1,27] The strong attractive forces are the origin of the sub molecular resolution as further discussed below.

The conductances show the expected exponential distance dependence at large tip-molecule distances until a change in the slope indicates the transition from the tunneling range to contact (Fig. 1(g)). This transition occurs close to the maximal attractive force as observed for single atoms and other molecules before.[26,51–53] The conductance at contact formation of $\approx 0.1 \ldots 0.3\, G_0$ ($G_0 = 2e^2/h$) measured on the phenyl ring is an order of magnitude larger than at other positions consistent with the larger electronic density of states due to the phenyl π-orbitals.

Figures 1(d), (e), and (f) show constant-height maps of the current and the frequency-shift for three tip heights. While the shape in the current maps is similar for all distances probed, the frequency shift map evolves with decreasing tip–molecule distance. Sharp sub-molecular features are due to increasingly negative frequency shifts. They are observed at distances exceeding the distance of maximal attractive force as well as the maximal negative

frequency shift (Fig. S2(d)). This is different from previous works where the atomic resolution was achieved at maximal negative frequency shift.[1,8]

To interpret the experimental findings, density functional theory (DFT) calculations were performed (see section methods for more details). First, we focus on the adsorption of MBA on the Au(110)-(1 × 1) surface. Other thiols are known to bind to gold surfaces after dehydrogenation of the mercapto (–SH) group.[42,54–57] We consider a single molecule adsorbed on a position of the (5 × 4) unit cell. The adsorption energy without H at the apical S is −1.75 eV, which is lower than that obtained for the intact molecule (−1.43 eV) independent of the surface coverage. Therefore, our calculations indicate that MBA islands are comprised of thiolate radicals.

The arrangement of molecules on the surface is displayed in Figs. 2(a) and (b). The thiolate radical is adsorbed with the S-atom at a height $h = 1.95$ Å and with the phenyl ring enclosing an angle 10° with the Au substrate. While the S-Au bond favors an upright orientation, the van der Waals interaction is sufficiently strong to orient the molecule almost parallel to the surface. The calculated tilt angle increases slightly (to 11°) when dimers are considered.

For one thiolate adsorbed on the surface we have analyzed configurations with the phenyl ring parallel and perpendicular to the surface. In the case of four molecules adsorbed on the surface we have considered lying-down configurations. Different adsorption geometries with the S-head initially located on high-symmetry sites were explored. The total energy balance shows that the thiol adsorption takes place by the dehydrogenated S atom of the molecule.

Table 1 summarizes the adsorption energies per molecule of an upright (vertical) and a lying (horizontal) molecule, as well as of an adsorbed dimer. The van der Waals forces between the phenyl ring and the surface are maximal in the lying geometry. Compared to the upright orientation, the dispersion contribution to the adsorption energy, denoted vdW in Table 1, is doubled. It is hardly changed in the adsorbed dimer, which adsorbs rather flat on the surface.

Table 1: Adsorption energies per molecule in eV. The different columns correspond to the energies of an adsorbed molecule with an upright phenyl ring (vertical), an adsorbed molecule with its phenyl ring parallel to the surface (horizontal), and an adsorbed molecular dimer. The considered energies are the total adsorption energy, E_{total}, the contribution coming from the van der Waals interaction (vdW), the interaction energy between molecules due to the formation of H-bonds (O··H··O), and the contribution of the S-metal bond (S–Au).

	vertical	horizontal	in adsorbed dimer
E_{total}	–1.00	–1.75	–2.29
vdW	–0.59	–1.20	–1.38
O··H··O	–	–	–0.53
S–Au	–0.57	–0.57	–0.57

In many thiols, the S-metal bonding largely drives the adsorption of molecules on gold.[28,45,54,58] In the present case, however, this kind of bond accounts for only 25% of the molecular adsorption energy in dimers. To first approximation, MBA is adsorbed via the dispersion interaction while the S-metal bond introduces selectivity for a specific site. Indeed, the S atoms are located close to the short-bridge site of Au(110) and 1.95 Å away from the surface plane. This site specificity forces a zigzag structure of the aligning rows of dimers because dimers can only form compact structures if their S atoms adsorb to adjacent Au rows, Fig. 2(a). Otherwise, the steric repulsion between hydrogen atoms of adjacent MBA molecules would be too large.

A further important contribution to the dimer stability is due to hydrogen bonding. In gas phase, the formation energy of a dimer is -0.41 eV per molecule. It reduces to -0.55 eV for the intramolecular coordinates frozen. This value is very close to the energy due to the formation of H-bonds between molecules in adsorbed dimers, see Table 1, implying that the intramolecular geometries are largely fixed by the adsorption to the substrate.

On the Au surface, the energy due to hydrogen bond formation in dimers is comparable with that of the S-metal bond. As a result of these interactions the MBA molecules are fixed on both sides. The sulfur side binds to the Au substrate while the carboxylic group causes hydrogen bonding.

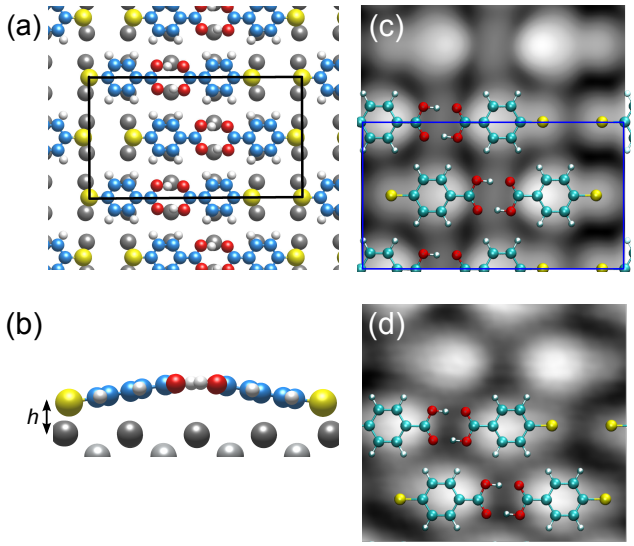

Figure 2: (a) Top and (b) side views of a relaxed molecular adlayer. The separation h between the S and Au atoms is indicated. (c) Simulated constant-current STM image (contours of constant local density of states, electron density: 1.5×10^{-12} electrons per nm^3), size: 2.1 nm $\times$ 2.1 nm. A ball-and-stick model of the molecular adlayer is overlaid. The black and blue boxes in (a) and (c) indicate the (5×4) unit cell. (d) Experimental constant-current image of an MBA island (2.1 nm $\times$ 1.8 nm, $V = 15$ mV, $I = 0.3$ nA) along with overlaid molecular structures.

Next the structure of the underlying Au surface is discussed. Overview images show dimer rows extending along the Au(110)-(2×1) rows (Fig. 1(h) and Fig. S1 of the Supporting Information (SI)). Due to the site-specificity of the S-Au bonds and the steric forces between MBA molecules, the dimers arrange themselves in a zigzag fashion, with adjacent dimers shifted by the lattice parameter a. This arrangement of dimer rows is incompatible with the (2×1) reconstruction of the Au substrate. We thus conclude that the reconstruction is lifted underneath the molecular rows in favor of a (1×1) pattern. This analysis and the above adsorption configuration are further supported by the good agreement between simulated (Tersoff-Hamann[59]) and experimental STM constant-current images, Figs. 2 (c) and (d), respectively. We suggest that the growth of MBA rows proceeds via the removal of atomic Au rows from the Au(110)-(2×1) reconstruction, which leads to the ideal (1×1) surface. This is consistent with the observations that fairly straight MBA dimer rows extend far into well-ordered (2×1) terraces and that smaller clusters of MBA grow on the next

higher Au terrace (Figs. 1(h) and S1). If the mechanism were the addition of Au adatoms (so filling the existing missing-row reconstruction), the adatoms would stem from the step edges and diffuse along the [$\bar{1}$10] direction.[60,61] In this case, the diffusion and addition of adatoms would stop as soon as the first row of MBA pairs adsorbs to the step edges. Hence, a large-island (as shown in Fig. S1) would not be expected. As described by Kühnle et al.,[62] the removal of a row atom becomes easier when an atom has already been extracted. Consequently, continued growth of an existing dimer row is more likely than the creation of new rows.

Single gold adatoms have been shown to direct the interaction between some thiol-based molecules.[54,56,58] In the present case, however, we did not observe evidence of adatom-mediated interaction. Indeed, the frequent detection of single dimer rows (red boxes in Fig. S1), which exhibit two S atoms per dimer at their sides, is difficult to reconcile with the presence adatoms that sulfur atoms would bond to. Moreover, no variation of the frequency shift is detected over the location of a hypothetical adatom (Figs. 1(c) and (f)). The STM images do not suggest the presence of a Au adatom between the S atoms of adjacent MBA molecules. However, image simulations based on the DFT calculations reveal that such an adatom, if present, would hardly be visible in STM images due to the small contrast of a gold adatom between two sulphur atoms. We therefore evaluated the energies of the (5×4) MBA overlayer with and without Au adatoms. Comparing the adsorption energy of MBA dimers on the Au(110)-(1×1) surface and a Au(110) surface with adatoms near the edge S-atom, we find the latter to be 0.37 eV/molecule less favorable. Our experimental data and calculations therefore do not favor adatoms as driving the formation of the molecular pattern.

To estimate the interactions due to covalent bonding between tip and molecule, we modelled the tip by a (111) pyramid of 10 Au atoms (see methods). The tip-sample distance was varied in steps of 0.5 Å and the molecules, the two topmost surface layers, and the tip apex atom were relaxed. The other layers of the tip were used to determine the force on

the tip. Furthermore, an electrostatic force between the electrical dipole of the tip[63,64] and the charge distribution of the molecules was taken into account. To evaluate the force on the molecule we assumed a point-dipole $D = 1$ Debye oriented along the axis normal to the surface.[64] The vertical force component is

$$F_z(\vec{r}) = -D\frac{d^2}{dz^2}V(\vec{r}), \tag{1}$$

where $V(\vec{r})$ is the electrostatic potential of the full system comprising the molecule and the surface.

Figure 3(a) shows the calculated forces between the pyramidal tip and the substrate at three sites: at an O atom, between the O atoms, and at the phenyl ring. The high symmetry of this model tip leads to a negligible dipolar moment in the tip, permitting us to isolate the electrostatic interactions using expression Eq. (1). The maximum of the electrostatic force on the oxygen atoms is also indicated for comparison.[65] The largest attractive force is exerted on the phenyl ring. The maximum occurs at a tip-sample distance of $d \sim 7.85$ Å i. e. ~ 0.6 Å closer to the substrate than the attractive maximum on the O atoms. These distances qualitatively agree with the experimental observation that the maximum attractive force is larger on the phenyl than on the O atoms and that it occurs at a reduced tip-surface distance d compared to the phenyl site (by 0.2 Å in the experimental data).

The force analysis shows that for $d > 9$ Å, the van der Waals interaction dominates the force between the molecule and the model tip. In this range, the tip is largely insensitive to the molecular structure. When the tip is brought closer to the molecule, the covalent interaction first sets in over the O atoms. Our model tip reproduces the enhanced attractive signal in AFM images over the oxygen atoms shown in Fig. 1(c) since the interaction is more attractive on the oxygen atoms than in between (Fig. 3(a)). A significant contribution to the signal over oxygen atoms comes from a mechanical deformation of the molecule, Fig. 3(b). The relatively small interaction of the oxygen groups with the surface allows for a motion of

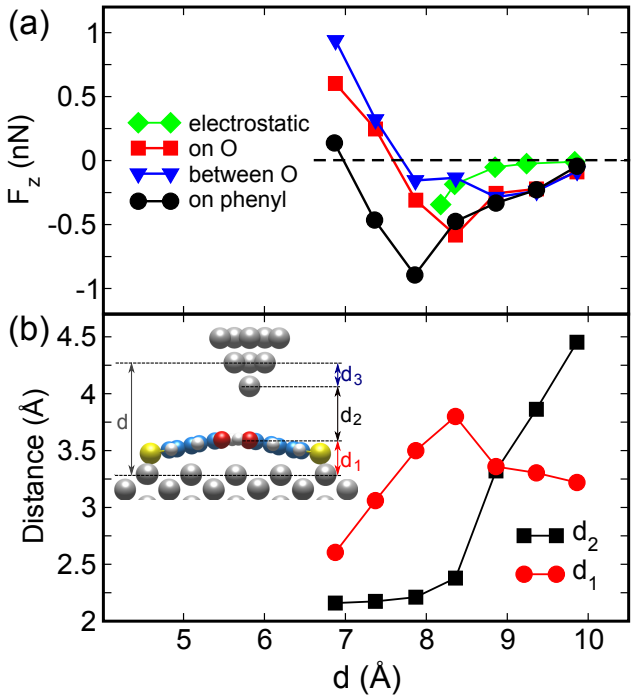

Figure 3: (a) Perpendicular component of the force between the pyramidal gold tip and the two MBA dimers on Au(111) versus the distance d between the top layer of the sample and the unrelaxed second layer of the tip as marked in the inset. The force was evaluated at three different sites: atop of an O atom (squares), between O atoms (triangles), and at the phenyl ring (circles), cf. Fig. 1(c). The electrostatic force on one of the O atoms is shown for comparison (diamonds). (b) Atomic displacement given by the distance between an oxygen atom of the molecular dimer and the top-most surface layer d_1 (red circles) or the tip apex d_2 (black squares). See inset for the definition of distances d, d_1 and d_2. The position of the tip apex atom d_3 varies less than 0.08 Å within the depicted distance range, starting at $d_3 =$ 2.19 Å for $d =$9.86 Å.

the oxygen atoms to the tip (see also Fig. S5). At the largest attractive force (tip–surface distance of ~ 8.4 Å, red squares in Fig. 3(a)) the displacement of the oxygen atom to the tip (black squares in Fig. 3(b)) is larger than the variation of d. This leads to a marked non-linear behavior of the curves in Fig. 3(b). The oxygen distance to the tip decreases by ~ 1 Å, roughly 0.5 Å more than expected from a rigid behavior following the motion of the tip. In comparison, the tip-apex atom is stiffer, moving less than 0.08 Å from its equilibrium distance, and basically following the variation of d. The oxygen motion towards the tip apex takes place in a very narrow region of $d \sim 8.4 \ldots 8.9$ Å. Experimentally, we find a smoother variation of the frequency shift between two oxygen atoms of different molecules than between oxygen atoms of the same molecule (Fig. S4(b)). This indicates that relaxations are stronger when the tip is positioned between oxygen atoms of the same molecule.

The sharp response of the O atoms to the position of the tip explains the enhanced corrugation of over the O atoms. The contrast in AFM images (starting at $\Delta z = -0.8$ Å, Figs. 1(c) to (f)) is observed beyond the maximal attractive force above the oxygen atoms. According to the calculated force curves in Fig. 3(b), $\Delta z = -0.8$ Å corresponds to a tip–molecule distance $d \sim 3.3$ Å. This is similar to the distance reported for atomic resolution imaging of C_{60} with a CO-functionalized tip.[8] Given the absence of dipolar contributions from our model tip, we conclude that the sharp features above the oxygen atoms in the AFM images (Fig. 1(c)) are mainly due to the covalent interaction with the tip enhanced by the motion of the carboxylic group during the approach of the tip. This is different compared to a recent work that used a CO-functionalized tip to image a molecule with carboxylic groups.[24] Sub-molecular contrast is observed on the oxygen atoms, but it is due to the repulsive electrostatic interaction between the partially negatively charged oxygen atoms of both the CO and the carboxylic group. Although we cannot rule out some contribution from electrostatic interactions between the oxygen atoms and metallic tips of more than 1 Debye of dipolar moment, see diamonds in Fig. 3(a) and Fig. S6, our calculations show that the covalent interaction is the dominating one.

As to the position above the phenyl rings, where the maximum force occurs (Fig.1(g)), the calculations show that the electrostatic and van der Waals forces are outgrown by the covalent contribution for distances shorter than 9 Å. Thus, the large contrast measured over the phenyl ring is due to the covalent interaction between the metallic tip and the π-electron system.

In conclusion, we combined STM and AFM measurements with DFT calculations aspects of the geometry and interactions of self-assembled layer of MBA on Au(110) are unraveled. The attractive interaction between MBA molecules and the metallic tip leads to remarkably sharp features in frequency-shift AFM images above the oxygen atoms and also above the phenyl ring. DFT simulations involving a reactive tip terminated in a single metallic atom explain the results. The large effect of the phenyl ring is attributed to the covalent interaction between the tip and the π-electron system of the molecule. The corrugation over the O atoms has both electrostatic and covalent contribution with the latter being the dominating one. In addition, relaxations of the oxygen atoms towards the tip by $\sim$ 0.5 Å are found due to the weak oxygen-surface interaction. These results show the complementarity of STM and AFM in analysing molecular structures, and highlight the usefulness of metallic tips to obtain high-resolution frequency-shift maps.

MBA adsorbs almost flat (angle of 11°) on Au(110) and forms dimers owing to hydrogen bonding of the carboxylic groups. The Au(110)-(2×1) reconstruction is lifted and we found no evidence of Au adatoms being involved in binding the MBA molecules. Most of the adsorption energy is due to the dispersion interaction of π-electrons of the phenyl ring with the metal substrate while the thiol-Au bond contributes $\approx$ 25%, enough to pin the dimers to short-bridge sites of the ideal Au(110) substrate. This adsorption site together with the steric repulsion between molecular dimers leads to a zigzag pattern.

Methods

STM and AFM measurements

Our measurements were performed in a combined STM/AFM setup in ultra-high vacuum at 5 K. Au(110) surfaces were cleaned by Ar^+ sputtering and annealing to 750 K. 4-Mercaptobenzoic acid molecules (Sigma Aldrich, purity 99 %) were sublimated from a molybdenum crucible onto the Au(110) substrate that was kept at a slightly elevated temperature (between 30 °C and 60 °C). STM tips were prepared by repeated indenting them into the Au(110) substrate at elevated voltages. Whenever instabilities occurred during data acquisition that suggested the presence of a molecule at the tip, the tip-shaping procedure was repeated until stable conditions were obtained[65] . For AFM measurements, a non-contact frequency-modulation mode was used with a Q-plus sensor[66] oscillating at its resonance frequency of ≈ 23 kHz at a constant amplitude $A = 0.4$ Å. A W tip was attached to the free prong of the tuning fork.[65] The current and the frequency shift were simultaneously measured. To approximately remove the van der Waals contribution of the bulk tip from the frequency-shift data, distant-dependent measurements recorded on the bare Au(110) surface were subtracted from those taken on MBA molecules. The short-range force and instantaneous conductance and were obtained by deconvolution following Refs. 67 and 68, respectively.[65]

DFT calculations

All calculations were carried out with the VASP[69] code by solving the one-electron Kohn-Sham equation within the generalized gradient approximation proposed by Perdew, Burke, and Ernzerhof (PBE)[70] to treat electronic exchange and correlation. Dispersion corrections are included through the scheme proposed by Tkatchenko and Scheffler.[71] We used a plane wave basis set and the projected augmented wave (PAW) method[72] implemented in VASP with an energy cut-off of 400 eV. The Au(110) surface is represented by a five-layer slab and

in all calculations we allowed the relaxation of the substrate atoms in the two top-most metal layers as well as all the atoms of the adsorbates (the substrate atoms in the three bottom layers were kept fixed in their bulk equilibrium positions). We assumed that adsorption takes place on the perfect Au(110) surface due to the lower calculated adsorption energy (notice that it is a negative quantity) compared to that on the reconstructed surface. All geometry optimizations were carried out until the forces on every mobile atom were smaller than 0.01 eV/Å. The Brillouin zone sampling was carried out according to the Monkhorst and Pack method with a $3 \times 5 \times 1$ mesh of the Brillouin zone.

Acknowledgement

Financial support from the Deutsche Forschungsgemeinschaft via the SFB 677 is gratefully acknowledged. ICN2 acknowledges support from the Severo Ochoa Program (MINECO, Grant SEV-2013-0295). P.A. acknowledges the MINCyT (project PICT Bicentenario 1962), CONICET (project PIP 0272), and UNR (project PID 19/I375) and the CCT-Rosario Computational Center.

Supporting Information Available

Overview STM image of a MBA island, details on the distant-dependent measurements, tip preparation, cross-sectional profiles, asymmetries and dissipation in AFM images, as well as details on the calculation of the adsorption energies, the covalent and the electrostatic forces, and the relaxed geometries of tip-molecule junctions. This material is available free of charge via the Internet at `http://pubs.acs.org/`.

References

(1) Gross, L.; Mohn, F.; Moll, N.; Liljeroth, P.; Meyer, G. The Chemical Structure of a Molecule Resolved by Atomic Force Microscopy. *Science* **2009**, *325*, 1110–1114.

(2) Oteyza, D. G. d.; Gorman, P.; Chen, Y.-C.; Wickenburg, S.; Riss, A.; Mowbray, D. J.; Etkin, G.; Pedramrazi, Z.; Tsai, H.-Z.; Rubio, A. et al. Direct Imaging of Covalent Bond Structure in Single-Molecule Chemical Reactions. *Science* **2013**, *340*, 1434–1437.

(3) Zhang, J.; Chen, P.; Yuan, B.; Ji, W.; Cheng, Z.; Qiu, X. Real-Space Identification of Intermolecular Bonding with Atomic Force Microscopy. *Science* **2013**, *342*, 611–614.

(4) Schuler, B.; Meyer, G.; Peña, D.; Mullins, O. C.; Gross, L. Unraveling the Molecular Structures of Asphaltenes by Atomic Force Microscopy. *J. Am. Chem. Soc.* **2015**, *137*, 9870–9876.

(5) Ernst, K.-H.; Baumann, S.; Lutz, C. P.; Seibel, J.; Zoppi, L.; Heinrich, A. J. Pasteur's Experiment Performed at the Nanoscale: Manual Separation of Chiral Molecules, One by One. *Nano Lett.* **2015**, *15*, 5388–5392.

(6) Mönig, H.; Hermoso, D. R.; Díaz Arado, O.; Todorović, M.; Timmer, A.; Schüer, S.; Langewisch, G.; Pérez, R.; Fuchs, H. Submolecular Imaging by Noncontact Atomic Force Microscopy with an Oxygen Atom Rigidly Connected to a Metallic Probe. *ACS Nano* **2016**, *10*, 1201–1209.

(7) Pawlak, R.; Kawai, S.; Fremy, S.; Glatzel, T.; Meyer, E. High-Resolution Imaging of C_{60} Molecules using Tuning-Fork-Based Non-Contact Atomic Force Microscopy. *J. Phys.: Condens. Matter* **2012**, *24*, 084005.

(8) Gross, L.; Mohn, F.; Moll, N.; Schuler, B.; Criado, A.; Guitian, E.; Pena, D.; Gourdon, A.; Meyer, G. Bond-Order Discrimination by Atomic Force Microscopy. *Science* **2012**, *337*, 1326–1329.

(9) Moreno, C.; Stetsovych, O.; Shimizu, T. K.; Custance, O. Imaging Three-Dimensional Surface Objects with Submolecular Resolution by Atomic Force Microscopy. *Nano Lett.* **2015**, *15*, 2257–2262.

(10) Hauptmann, N.; González, C.; Mohn, F.; Gross, L.; Meyer, G.; Berndt, R. Interactions between two C_{60} Molecules measured by Scanning Probe Microscopies. *Nanotechnology* **2015**, *26*, 445703.

(11) Riss, A.; Wickenburg, S.; Gorman, P.; Tan, L. Z.; Tsai, H.-Z.; de Oteyza, D. G.; Chen, Y.-C.; Bradley, A. J.; Ugeda, M. M.; Etkin, G. et al. Local Electronic and Chemical Structure of Oligo-Acetylene Derivatives Formed Through Radical Cyclizations at a Surface. *Nano Lett.* **2014**, *14*, 2251–2255.

(12) Hapala, P.; Kichin, G.; Wagner, C.; Tautz, F. S.; Temirov, R.; Jelínek, P. Mechanism of High-Resolutions STM/AFM Imaging with Functionalized Tips. *Phys. Rev. B: Condens. Matter Mater. Phys.* **2014**, *90*, 085421.

(13) Hapala, P.; Temirov, R.; Tautz, F. S.; Jelínek, P. Origin of High-Resolution IETS-STM Images of Organic Molecules with Functionalized Tips. *Phys. Rev. Lett.* **2014**, *113*, 226101.

(14) Mohn, F.; Repp, J.; Gross, L.; Meyer, G.; Dyer, M. S.; Persson, M. Reversible Bond Formation in a Gold-Atom/Organic-Molecule Complex as a Molecular Switch. *Phys. Rev. Lett.* **2010**, *105*, 266102.

(15) Gross, L.; Mohn, F.; Moll, N.; Meyer, G.; Ebel, R.; Abdel-Mageed, W. M.; Jaspars, M. Organic Structure Determination using Atomic-Resolutionen Scanning Probe Microscopy. *Nature Chem.* **2010**, *2*, 821–825.

(16) Pavliček, N.; Fleury, B.; Neu, M.; Niedenführ, J.; Herranz-Lancho, C.; Ruben, M.; Repp, J. Atomic Force Microscopy Reveals Bistable Configurations of

Dibenzo[a,h]thianthrene and their Interconversion Pathway. *Phys. Rev. Lett.* **2012**, *108*, 086101.

(17) Hanssen, K. Ø.; Schuler, B.; Williams, A. J.; Demissie, T. B.; Hansen, E.; Andersen, J. H.; Svenson, J.; Blinov, K.; Repisky, M.; Mohn, F. et al. A Combined Atomic Force Microscopy and Computational Approach for the Structural Elucidation of Breitfussin A and B: Highly Modified Halogenated Dipeptides from Thuiaria Breitfussi. *Angew. Chem., Int. Ed.* **2012**, *51*, 12238–12241.

(18) Albrecht, F.; Neu, M.; Quest, C.; Swart, I.; Repp, J. Formation and Characterization of a Molecule–Metal–Molecule Bridge in Real Space. *J. Am. Chem. Soc.* **2013**, *135*, 9200–9203.

(19) Sweetman, A. M.; Jarvis, S. P.; Sang, H.; Lekkas, I.; Rahe, P.; Wang, Y.; Wang, J.; Champness, N. R.; Kantorovich, L.; Moriarty, P. Mapping the Force Field of a Hydrogen-Bonded Assembly. *Nat. Commun.* **2014**, *5*, 3931.

(20) Schuler, B.; Liu, S.-X.; Geng, Y.; Decurtins, S.; Meyer, G.; Gross, L. Contrast Formation in Kelvin Probe Force Microscopy of Single π-Conjugated Molecules. *Nano Lett.* **2014**, *10*, 739–746.

(21) Hämäläinen, S. K.; van der Heijden, N.; van der Lit, J.; den Hartog, S.; Liljeroth, P.; Swart, I. Intermolecular Contrast in Atomic Force Microscopy Images without Intermolecular Bonds. *Phys. Rev. Lett.* **2014**, *113*, 186102.

(22) Kawai, S.; Sadeghi, A.; Xu, F.; Peng, L.; Orita, A.; Otera, J.; Goedecker, S.; Meyer, E. Extended Halogen Bonding between Fully Fluorinated Aromatic Molecules. *ACS Nano* **2015**, *9*, 2574–2583.

(23) Iwata, K.; Yamazaki, S.; Mutombo, P.; Hapala, P.; Ondráček, M.; Jelínek, P.; Sugimoto, Y. Chemical Structure Imaging of a Single Molecule by Atomic Force Microscopy at Room Temperature. *Nat. Commun.* **2015**, *6*, 7766.

(24) van der Lit, J.; Di Cicco, F.; Hapala, P.; Jelínek, P.; Swart, I. Submolecular Resolution Imaging of Molecules by Atomic Force Microscopy: The Influence of the Electrostatic Force. *Phys. Rev. Lett.* **2016**, *116*, 096102.

(25) Schwarz, A.; Köhler, A.; Grenz, J.; Wiesendanger, R. Detecting the Dipole Moment of a Single Carbon Monoxide Molecule. *Appl. Phys. Lett.* **2014**, *105*, 011606.

(26) Caffrey, N. M.; Buchmann, K.; Hauptmann, N.; Lazo, C.; Ferriani, P.; Heinze, S.; Berndt, R. Competing Forces during Contact Formation between a Tip and a Single Molecule. *Nano Lett.* **2015**, *15*, 5156–5160.

(27) Ellner, M.; Pavliček, N.; Pou, P.; Schuler, B.; Moll, N.; Meyer, G.; Gross, L.; Peréz, R. The Electric Field of CO Tips and its Relevance for Atomic Force Microscopy. *Nano Lett.* **2016**, *16*, 1974–1980.

(28) Love, J. C.; Estroff, L. A.; Kriebel, J. K.; Nuzzo, R. G.; Whitesides, G. M. Self-Assembled Monolayers of Thiolates on Metals as a Form of Nanotechnology. *Chem. Rev.* **2005**, *105*, 1103–1170.

(29) Camillone, N.; Leung, T. Y. B.; Schwartz, P.; Eisenberger, P.; Scoles, G. Chain Length Dependence of the Striped Phases of Alkanethiol Monolayers Self-Assembled on Au(111): An Atomic Beam Diffraction Study. *Langmuir* **1996**, *12*, 2737–2746.

(30) Gerlach, R.; Polanski, G.; Rubahn, H.-G. Structural Manipulation of Ultrathin Organic Films on Metal Surfaces: The Case of Decane Thiol/Au(111). *Appl. Phys. A* **1997**, *65*, 375–377.

(31) Staub, R.; Toerker, M.; Fritz, T.; Schmitz-Hübsch, T.; Sellam, F.; Leo, K. Flat Lying Pin-Stripe Phase of Decanethiol Self-Assembled Monolayers on Au(111). *Langmuir* **1998**, *14*, 6693–6698.

(32) Kondoh, H.; Kodama, C.; Sumida, H.; Nozoye, H. Molecular Processes of Adsorption and Desorption of Alkanethiol Monolayers on Au(111). *J. Chem. Phys.* **1999**, *111*, 1175–1184.

(33) Poirier, G. E. Coverage-Dependent Phases and Phase Stability of Decanethiol on Au(111). *Langmuir* **1999**, *15*, 1167–1175.

(34) Shimada, T.; Kondoh, H.; Nakai, I.; Nagasaka, M.; Yokota, R.; Amemiya, K.; Ohta, T. Structural Study of Hexanethiolate on Au(111) in the 'Striped' Phase. *Chem. Phys. Lett.* **2005**, *406*, 232–236.

(35) Poirier, G. E.; Pylant, E. D. The Self-Assembly Mechanism of Alkanethiols on Au(111). *Science* **1996**, *272*, 1145–1148.

(36) Ulman, A. Formation and Structure of Self-Assembled Monolayers. *Chem. Rev.* **1996**, *96*, 1533–1554.

(37) Schreiber, F. Structure and Growth of Self-Assembling Monolayers. *Proc. Natl. Acad. Sci. U. S. A.* **2000**, *65*, 151–257.

(38) Schreiber, F. Self-Assembled Monolayers: From Simple Model Systems to Biofunctionalized Interfaces. *J. Phys.: Condens. Matter* **2004**, *16*, R881–R900.

(39) Vericat, C.; Vela, M. E.; Salvarezza, R. C. Self-Assembled Monolayers of Alkanethiols on Au(111): Surface Structures, Defects and Dynamics. *Phys. Chem. Chem. Phys.* **2005**, *7*, 3258–3268.

(40) Love, J. C.; Estroff, L. A.; Kriebel, J. K.; Nuzzo, R. G.; Whitesides, G. M. Self-Assembled Monolayers of Thiolates on Metals as a Form of Nanotechnology. *Chem. Rev.* **2005**, *105*, 1103–1170.

(41) Woodruff, D. P. The Interface Structure of n-Alkylthiolate Self-Assembled Monolayers on Coinage Metal Surfaces. *Phys. Chem. Chem. Phys.* **2008**, *10*, 7211–7221.

(42) Häkkinen, H. The Gold-Sulfur Interface at the Nanoscale. *Nat. Chem.* **2012**, *4*, 443–455.

(43) Jadzinsky, P. D.; Calero, G.; Ackerson, C. J.; Bushnell, D. A.; Kornberg, R. D. Structure of a Thiol Monolayer-Protected Gold Nanoparticle at 1.1 Å Resolution. *Science* **2007**, *318*, 430–433.

(44) Walter, M.; Akola, J.; Lopez-Acevedo, O.; Jadzinsky, P. D.; Calero, G.; Ackerson, C. J.; Whetten, R. L.; Grönbeck, H.; Häkkinen, H. A Unified View of Ligand-Protected Gold Clusters as Superatom Complexes. *Proc. Natl. Acad. Sci. U. S. A.* **2008**, *105*, 9157–9162.

(45) Pensa, E.; Cortes, E.; Corthey, G.; Carro, P.; Vericat, C.; Fonticelli, M. H.; Benitez, G.; Rubert, A. A.; Salvarezza, R. C. The Chemistry of the Sulfur-Gold Interface: In Search of a Unified Model. *Acc. Chem. Res.* **2012**, *45*, 1183–1192.

(46) Pensa, E.; Rubert, A. A.; Benitez, G.; Carro, P.; Orive, A. G.; Creus, A. H.; Salvarezza, R. C.; Vericat, C. Are 4-Mercaptobenzoic Acid Self Assembled Monolayers on Au(111) a Suitable System to Test Adatom Models? *J. Phys. Chem. C* **2012**, *116*, 25765–25771.

(47) Lee, J. R. I.; Willey, T. M.; Nilsson, J.; Terminello, L. J.; De Yoreo, J. J.; van Buuren, T. Effect of Ring Substitution Position on the Structural Conformation of Mercaptobenzoic Acid Self-Assembled Monolayers on Au(111). *Langmuir* **2006**, *22*, 11134–11141.

(48) Barriet, D.; Yam, C. M.; Shmakova, O. E.; Jamison, A. C.; Lee, T. R. 4-Mercaptophenylboronic Acid SAMs on Gold: Comparison with SAMs Derived from Thiophenol, 4-Mercaptophenol, and 4-Mercaptobenzoic Acid. *Langmuir* **2007**, *23*, 8866–8875.

(49) Schäfer, A. H.; Seidel, C.; Chi, L.; Fuchs, H. STM Investigations of Thiol Self-Assembled Monolayers. *Adv. Mater* **1998**, *10*, 839–842.

(50) Koslowski, B.; Tschetschetkin, A.; Maurer, N.; Ziemann, P. 4-Mercaptopyridine on Au(111): A Scanning Tunneling Microscopy and Spectroscopy Study. *Phys. Chem. Chem. Phys.* **2011**, *13*, 4045–4050.

(51) Frederiksen, T.; Lorente, N.; Paulsson, M.; Brandbyge, M. From Tunneling to Contact: Inelastic Signals in an Atomic Gold Junction from First Principles. *Phys. Rev. B* **2007**, *75*, 235441.

(52) Ternes, M.; González, C.; Lutz, C. P.; Hapala, P.; Giessibl, F. J.; Jelínek, P.; Heinrich, A. J. Interplay of Conductance, Force, and Structural Change in Metallic Point Contacts. *Phys. Rev. Lett.* **2011**, *106*, 016802.

(53) Hauptmann, N.; Mohn, F.; Gross, L.; Meyer, G.; Frederiksen, T.; Berndt, R. Force and Conductance during Contact Formation to a C_{60} Molecule. *New J. Phys.* **2012**, *14*, 073032.

(54) Maksymovych, P.; Sorescu, D. C.; Yates, J. T. Gold-Adatom-Mediated Bonding in Self-Assembled Short-Chain Alkanethiolate Species on the Au(111) Surface. *Phys. Rev. Lett.* **2006**, *97*, 146103.

(55) Gonzalez-Lakunza, N.; Lorente, N.; Arnau, A. Chemisorption of Sulfur and Sulfur-Based Simple Molecules on Au(111). *J. Phys. Chem. C* **2007**, *111*, 12383–12390.

(56) Voznyy, O.; Dubowski, J. J.; Yates, J. T.; Maksymovych, P. The Role of Gold Adatoms and Stereochemistry in Self-Assembly of Methylthiolate on Au(111). *J. Am. Chem. Soc.* **2009**, *131*, 12989–12993.

(57) Li, F.; Tang, L.; Gao, J.; Zhou, W.; Guo, Q. Adsorption and Electron-Induced Dissociation of Ethanethiol on Au(111). *Langmuir* **2012**, *28*, 11115–11120.

(58) Maksymovych, P.; Voznyy, O.; Dougherty, D. B.; Sorescu, D. C.; Yates Jr., J. T. Gold

Adatom as a Key Structural Component in Self-Assembled Monolayers of Organosulfur Molecules on Au(111). *Proc. Natl. Acad. Sci. U. S. A.* **2010**, *85*, 206–240.

(59) Tersoff, J.; Hamann, D. R. Theory of the Scanning Tunneling Microscope. *Phys. Rev. B* **1985**, *31*, 805–813.

(60) Kuipers, L.; Hoogeman, M. S.; Frenken, J. W. M. Step Dynamics on Au(110) studied with a High-Temperature, High-Speed Scanning Tunneling Microscope. *Phys. Rev. Lett.* **1993**, *71*, 3517–3520.

(61) Rost, M. J.; van Albada, S. B.; Frenken, J. W. M. How Asymmetric Islands become Symmetric. *Phys. Rev. Lett.* **2001**, *86*, 5938–5941.

(62) Kühnle, A.; Molina, L. M.; Linderoth, T. R.; Hammer, B.; Besenbacher, F. Growth of Unidirectional Molecular Rows of Cysteine on Au (110) Driven by Adsorbate-Induced Surface Rearrangements. *Phys. Rev. Lett.* **2004**, *93*, 086101.

(63) Teobaldi, G.; Lämmle, K.; Trevethan, T.; Watkins, M.; Schwarz, A.; Wiesendanger, R.; Shluger, A. L. Chemical Resolution at Ionic Crystal Surfaces Using Dynamic Atomic Force Microscopy with Metallic Tips. *Phys. Rev. Lett.* **2011**, *106*, 216102.

(64) Gao, D. Z.; Grenz, J.; Watkins, M. B.; F. F, C.; Schwarz, A.; Wiesendanger, R.; Shluger, A. L. Using Metallic Noncontact Atomic Force Microscope Tips for Imaging Insulators and Polar Molecules: Tip Characterization and Imaging Mechanisms. *ACS Nano* **2014**, *8*, 5339–5351.

(65) See the Supporting Information for further Details.

(66) Giessibl, F. J. High-Speed Force Sensor for Force Microscopy and Profilometry Utilizing a Quartz Tuning Fork. *Appl. Phys. Lett.* **1998**, *73*, 3956–3958.

(67) Sader, J. E.; Jarvis, S. P. Accurate Formulas for Interaction Force and Energy in Frequency Modulation Force Spectroscopy. *Appl. Phys. Lett.* **2004**, *84*, 1801–1803.

(68) Sader, J. E.; Sugimoto, Y. Accurate Formula for Conversion of Tunneling Current in Dynamic Atomic Force Spectroscopy. *Appl. Phys. Lett.* **2010**, *97*, 043502.

(69) Kresse, G.; Furthmüller, J. Efficiency of Ab-Initio Total Energy Calculations for Metals and Semiconductors using a Plane-Wave Basis Set. *Comput. Mater. Sci.* **1996**, *6*, 15.

(70) Perdew, J. P.; Burke, K.; Ernzerhof, M. Generalized Gradient Approximation made Simple. *Phys. Rev. Lett.* **1996**, *77*, 3865–3868.

(71) Tkatchenko, A.; Scheffler, M. Accurate Molecular Van Der Waals Interactions from Ground-State Electron Density and Free-Atom Reference Data. *Phys. Rev. Lett.* **2009**, *102*, 073005.

(72) Kresse, G.; Joubert, D. From Ultrasoft Pseudopotentials to the Projector Augmented-Wave Method. *Phys. Rev. B* **1999**, *59*, 1758–1775.